Environmental Science and Pollution Research (2024) 31:46498–46512
https://doi.org/10.1007/s11356-023-26261-5

SMART NANOMATERIALS FOR HEALTHCARE AND ENVIRONMENTAL APPLICATIONS: PERSPECTIVES IN NANOTOXICOLOGY

Improved anti-diabetic and anticancer activities of green synthesized CuO nanoparticles derived from *Tabernaemontana divaricate* leaf extract

Manonmani Raju[1] · Balaji Parasuraman[2] · Palanisamy Govindasamy[2] · Pazhanivel Thangavelu[2] · Sasikumar Duraisamy[1]

Received: 6 December 2022 / Accepted: 28 February 2023 / Published online: 11 March 2023

Abstract

Copper oxide nanoparticles (CuO NPs) are among the most commonly employed nanoparticle materials owing to their antibacterial qualities, although their primary mechanism of action (MOA) is still not completely understood. CuO NPs are synthesized in this study using leaf extract of *Tabernaemontana divaricate* (TDCO3), and they are then analyzed using XRD, FT-IR, SEM, and EDX analysis. The zone of inhibition of TDCO3 NPs against both gram-positive (G^+) *B. subtilis* and gram-negative (G^-) *K. pneumoniae* bacteria was 34 mm and 33 mm, respectively. Furthermore, Cu^{2+}/Cu^+ ions promote reactive oxygen species and electrostatically bind with the negatively charged teichoic acid in the bacterial cell wall. The anti-inflammatory and anti-diabetics analysis was conducted using standard BSA denaturation and α-amylase inhibition technique with cell inhibition values of 85.66 and 81.18% for TDCO3 NPs. Additionally, the TDCO3 NPs delivered prominent anticancer activity with the lowest IC_{50} value 18.2 µg/mL in the MTT assay technique against HeLa cancer cells.

Keywords Tabernaemontana divaricate · CuO NPs · HeLa cancer cells · BSA denaturation · α-amylase

Introduction

Nano-biotechnology was an interdisciplinary field that fell between material science and bionanotechnology (Sarmast and Salehi 2016). In comparison to bulk materials, nanomaterials have unique features that lend themselves to use in the fields of material science, physics, chemistry, environmental clean-up, optics, biology, biomedicine, and semiconductors (Hasnidawani et al. 2016; Mirzaei and Darroudi 2017; Darvishi et al. 2019). Due to their enormous surface area, small sizes, exceptional reactivity, and free-hanging connections, nanoparticles (NPs) possess astonishing and alluring features. These particles are the consequence of an exponential increase in global spending on nanotechnology and nanoscience research (Zhao et al. 2020; Shojaei et al. 2021). Metal oxide NPs have been produced utilizing a variety of processes, including thermal decomposition, solution phase, sonochemical, solvothermal, microwave irradiation, ionic liquid assisted, electrochemical, spray pyrolysis, and sol-gel method, according to numerous papers up to this point (Sodipo and Aziz 2016; dos Santos Araújo et al. 2019). But

Highlights
- The CuO NPs were synthesized via a greener method utilizing Tabernaemontana divaricate leaf extract as a reducing and capping agent.
- Potential anticancer activity against HeLa cancer cells was observed with low IC50 = 18.2µg/mL concentration.
- The anti-inflammatory action possesses higher cell inhibition (85.55%).
- The TDCO3 NPs effectively inhibit α-amylase (81.18%) rendering prominent anti-diabetic activity.

Responsible Editor: George Z. Kyzas

✉ Sasikumar Duraisamy
sasikumarkd@gmail.com

[1] PG and Research Department of Physics, Arignar Anna Government Arts College, Namakkal, Tamil Nadu 637002, India

[2] Smart Materials Laboratory, Department of Physics, Periyar University, Salem, Tamil Nadu 636011, India

regrettably, the aforementioned physical and chemical techniques have unique drawbacks including being very expensive and unpleasant (Taghizadeh et al. 2021). The search for a practical and environmentally friendly approach to NPs synthesis led to the development of greener methods. Traditional plant extraction techniques, such as capping, natural reducing, and stabilizing agents, have made significant advancements toward a successful green synthesis process (Sathiyavimal et al. 2021; Waris et al. 2021). Attributed to the prevalence of phytochemicals such as phenolic compounds, flavonoids, alkaloids, organic acids, terpenoids, and others, the process that is mediated by plants is quicker and displays excellent biological activity (Mahendiran et al. 2017; Rehana et al. 2017; Król et al. 2019). Particularly, the use of common medicinal plants results in the creation of substitute medications to treat a variety of illnesses such as bacterial infections, inflammations, diabetes, malignancies, and viral infections (Singh et al. 2020a, b).

T. divaricata is a member of the apocynaceous family and is both a medicinal and cosmetic plant that possesses anti-infection, antiparasitic, antibacterial, antifungal, and anti-inflammatory properties in its crude extract T Chandani (in Hindi), Nandibatle (in Kannada), Crepe Jasmine (in English), Kutampale (in Malayalam), Nandivardhanamu (in Telugu), and Nandhiyavattam are some of its other names (Tamil) (Sivaraj et al. 2014). It is widely distributed in Bangladesh, South Asia, and India and has dichotomous branches that contain herbs or young trees. It produces stunning white fragrant flowers that can occasionally be seen throughout the year (KALAIMAGAL C 2019). The leaves are streamlined, substantial, deep green in colour, and rich in phytochemicals such alkaloids, tannins, flavonoids, phytosterols, phenols, terpenes, and carbohydrates, *T. divaricata* leaf aqueous extract is used to make herbal medicines (Umamaheswari 2015; Raja et al. 2018). It is well known that plants produce flavonoids in response to microbial diseases. Numerous metal oxide nanoparticles such as CuO (Ananda Murthy et al. 2021), ZnO (Muthuvel et al. 2020), TiO_2 (Narayanan et al. 2021), NiO (Anand et al. 2020), CdO (Gowri et al. 2018), and Co_3O_4 (Kainat et al. 2021) were reported in previous literature for their unique properties and applications. There have been a lot of studies on expensive materials like gold and silver NPs (Rafique et al. 2019), but there have not been sufficient papers on copper nanoparticles presently. According to their biocidal and antibacterial ability against several infections that are resistant to commercially available antimicrobial treatments, copper oxide (CuO) nanoparticles have received considerable attention (Li et al. 2021) (Kumar et al. 2015; Sharmila et al. 2016). By customizing the surfaces of antimicrobial compounds with CuO nanomaterials, the nanosystem built with CuO is not only employed for treating infections but also for detecting pathogens (Jadhav et al. 2018). As a result, its features pave the way for the creation of smart drug delivery systems. Additionally, the CuO metal oxides used to make the organic and inorganic nanocompounds have special qualities like excellent thermal and electrical conductivity, resilience at high temperatures, and high mechanical strength. Also, in the production of superconductors, gas sensors, solar cells, lithography, and magnetoresistance materials, CuO NPs are widely used as a potential material (Jayakumarai et al. 2015; Jose Varghese et al. 2020). Utilizing human cervical (HeLa) cancer cells, the MTT test was used to evaluate the in vitro anticancer efficacy. The in vitro anti-inflammatory and antidiabetic studies were evaluated through BSA denaturation and α-amylase inhibition technique.

Materials and methods

Materials and chemicals required

The leaves of *Tabernaemontana divaricate* were collected from the local region of the southern part of Tamil Nadu, India. The chemicals and solvents used in this research work are of analytical grade. Especially, the highly pure copper (II) nitrate hexahydrate (Cu $(NO_3)_2$. xH_2O) was bought from Sigma-Aldrich and used as purchased without any such purifications. The Millipore water with ultrapure grade has been utilized throughout the experiment.

Green synthesis of copper oxide nanoparticle utilizing *Tabernaemontana divaricate* (bio-reductant) leaf extract

The leaves of *Tabernaemontana divaricate* (*T. divaricate*) were collected from the local region around Tamil Nadu. The freshly plugged leaves were weighed carefully at about 200 mg and milled sufficiently with an aid of a mortar and pestle. The grounded *T. divaricate* leaves were then suspended inside a round bottom flask containing 500 mL of water, and fitted in a Soxhlet apparatus under constant water flow. The set-up was heated till boiling, maintained for 6 h, and allowed to attain room temperature normally. Finally, the obtained extract was filtered using (Whatman no. 40) filter paper, leaving behind the residue. For later usage, the *T. divaricate* extract was gathered and kept in a refrigerator that was maintained at 5 °C.

The 50% of *T. divaricate* leaf extract was made up to a volume of 250 mL using DI water Cu $(NO_3)_2$. H_2O designated as the originator of Cu NPs was carefully weighed and prepared as copper nitrate solutions utilizing DI water. The prepared copper nitrate solutions were added dropwise to the *T. divaricate* leaf extract mixture with constant stirring for 5–6 h at 80 °C. The colour of the solution turns brown as an indication expressing the generation of copper

hydroxide ($Cu(OH)_2$) NPs. The obtained solid residue was washed with water and ethanol to remove impurities stuck with the NPs and eventually dried overnight at 80 °C. The schematic representation of CuO NPs synthesis with aid of *T. divaricate* leaf extract was displayed in Fig. 1, to explain the copper oxide formation with higher oxygen vacancies, CuO NPs composition, and structural phase change. The experiment was carried out under the same condition with varying amounts of Cu originator and named as follows, 1g (TDCO1), 3g (TDCO3), and 5g (TDCO5) respectively.

Physical characterization of synthesized copper oxide nanoparticles

Powder X-ray diffraction (X'pert PRO analytical diffractometer) with Cu Kα radiation (0.1541 nm) was employed to characterize the crystalline structure, size, and phase confirmation of the *T. divaricate* leaf extract–induced CuO NPs. Fourier transform infrared (FT-IR) spectroscopy (Perkin-Elmer 1725) was used to confirm the chemical bonding and functional groups of the nanoparticles. Scanning electron microscopy and elemental mapping (SEM, EV018 (CARL ZEISS)) were employed to characterize the nanoparticles average size and size distribution.

Antimicrobial activity

The Gram-positive, *Bacillus subtilis* (*B. subtilis*), and Gram-negative, *Klebsiella pneumonia* (*K. pneumonia*), two bacterial strains were used to test the synthesized CuO NPs antibacterial efficacy via agar well diffusion method (Tanna et al. 2015). On agar plates, 20 mL of bacterial culture broth was poured using sterile L-rods. The spread plates were left undisturbed for 10 min, and the wells (5 mm in dia.) were made using a sterile gel core. Three different concentrations of CuO NPs suspension (40, 50, and 60 µg/ml) and positive control (50 µg/ml) (Amoxicillin) were made and added to the wells on all plates with the aid of a micropipette. All of the plates were held at 7.3 pH and incubated at 37 °C for 24 h. The inhibition zone (IZ) was evaluated followed by incubation. Three replicates of each screening test were used, and the results were tabulated as mean ± SE (standard error).

Cell culture procedure and cytotoxicity evaluation (MTT assay method)

The National Centre for Cell Sciences (NCCS), located in Pune, India, is where the human cervical cancer cell type HeLa was acquired. The cells were kept in McCoy's media that was supplemented with FCS, 2mM l-glutamine, and balanced salt solution (BSS), 0.1 mM non-essential amino acids, 1 mM sodium pyruvate, 2 mM l-glutamine, 10 mM (4-(2-hydroxyethyl)-1piperazineethane, and 1.5 g/L glucose; furthermore, streptomycin and penicillin were made up to 1mL/L. The cells were kept at 37 °C in a 5% CO_2 environment. The test samples were applied to the cells in successive concentrations after 24 h. Firstly, they were dissolved in plain dimethyl sulfoxide (DMSO), and the sample solution was diluted with serum-free medium to twice the desired final maximum test concentration. To give a total of five sample concentrations, an additional four serial dilutions were made. These various sample dilutions were added in aliquots of 100 µL to the relevant

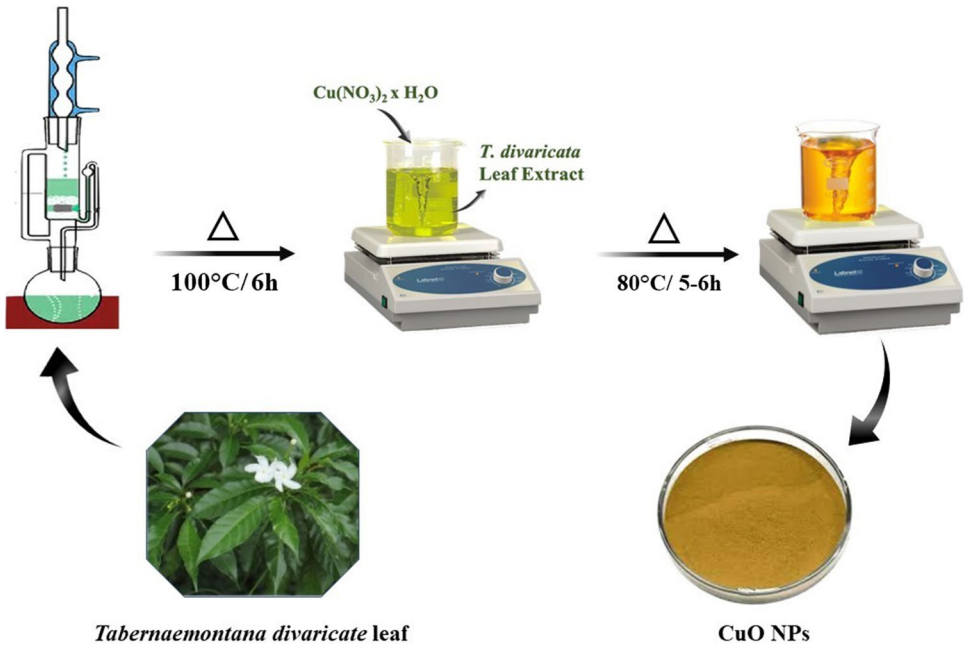

Fig. 1 Scheme on the synthesis of CuO NPs using *T. divaricate* leaf extract

wells that already had 100 µL of the medium, resulting in the necessary final sample concentrations. The plates were then incubated for an additional 48 h at 37 °C, 5% CO_2, 95% air, and 100% relative humidity after the addition of the sample (Khan et al. 2019). For all concentrations, triplicates were maintained and the medium containing no samples served as the control.

3-[4,5-dimethylthiazol-2-yl] 2,5-diphenyltetrazolium bromide (MTT) is a yellow-coloured water-soluble substance that was used to measure the amount of % viable cells, while the number of viable cells was directly correlated with the amount of formazan produced. The succinate-dehydrogenase is a mitochondrial enzyme that converts the MTT into purple-coloured formazan by cleaving the tetrazolium ring. After incubating for 48 h, each well was supplemented with 15 µL of MTT (5 mg/mL) in phosphate-buffered saline (PBS) and allowed to incubate for a period of 4 h at 37 °C.

In vitro anti-inflammatory activity

Utilizing the BSA denaturation procedure, the anti-inflammatory properties of the synthesized TDCO3 NPs were evaluated. In order to confirm the scavenging action, the standard reagent and the NPs were examined for albumin denaturation process inhibitions (Velsankar et al. 2020b). The minimal amount of dimethylformamide (DMF) was slowly dissolved in the crude extract and standard diclofenac sodium, which was then diluted and pH was altered to 7.4 using phosphate buffer. BSA solution (1 mM) was well mixed into 4 mL of the test solution that contains varied sample concentrations (50–500 g/mL). The mixture was then incubated for 15 min at 37 °C. The mixture was kept in a water bath at 70 °C for 30 min to induce the denaturation process.

Anti-diabetic activity

The α-amylase inhibition assay was used to assess the anti-diabetic activity of the synthesized TDCO3 NPs. In particular, 0.5 mg/mL of α-amylase, taken as the standard drug, was incubated for 10 min at 25 °C. The pH was adjusted to 6.9 with the addition of sodium phosphate buffer. The synthesized TDCO3 NPs was added to the above-prepared buffer solution at varying concentration (50–500 µg/mL) and left to incubate for 10 min at 25 °C. Afterward, starch (1%) was supplemented, and incubated at 100 °C inside a water bath, followed by the addition of dinitrosalicylic acid to control the enzymatic reaction. The UV-Visible spectrophotometer was used to read the absorbance at 540 nm after the mixture cooled down to normal temperature (Javed et al. 2017).

Result and discussion

Synthesis of *Tabernaemontana divaricate* leaf extract–mediated CuO NPs

The 3,7, 11, and 15-tetramethyl-2-hexadecane-1-ol and n-hexadecanoic acid phytochemicals present in the *T. divaricate* leaf extract promoted the formation of CuO NPs. Figure 2 illustrates the systematic approach to producing CuO NPs using the bio-reductant found in *T. divaricate* leaf extract. In brief, phytochemicals like 3, 7, 11, and 15-tetramethyl-2-hexadecane-1-ol are well known for their antibacterial and anti-inflammatory capabilities, while n-hexadecanoic acid. These phytochemicals act as bio-reductants because the hydroxyl (-OH) groups found in 3, 7, 11, and 15-tetramethyl-2-hexadecane-1-ol and n-hexadecanoic acid bind to copper nitrate to form a complex that triggers the nucleation process (Pandiyan et al. 2018). The Cu ions are then subjected to reduction ($Cu(OH)_2$) under steady stirring, heating, and changing into the desired shape. The phytochemicals act as a capping agent at this stage, transforming the metal hydroxide into the desired shape (Pandiyan et al. 2019). Additionally, the sample was heated to 80 °C to evaporate the H_2O content, resulting in the formation of CuO NPs. Overall, the interaction of naturally occurring phytochemicals and synthesized CuO NPs could significantly increase the cell mortality rate.

XRD analysis

The XRD method was used to determine the crystalline size and shape concerning microstrain for all synthesized *T. divaricate* leaf extract–mediated CuO NPs recorded in between the range of 20–80°. The XRD pattern in Fig. 3 a–c shows the formation of CuO monoclinic phases that matches with standard diffraction data (JCPDS No. 03-065-2309) (Wang et al. 2016). Major diffraction peaks in the spectra can be seen at 2θ = 32.34°, 35.79°, 39.44°, 61.19°, and 65.19°, respectively, which correspond to the (110), (111), (200), (022), and (113) crystal planes. In particular, other low intense peaks with lattice plane values of (112), (200), (312), and (116) were identified as the reflections of tetragonal-phased Cu_4O_3 NPs (JCPDS No. 033-0480) (Patzschke et al. 2021). As the weight percentage of copper precursors increases, the interference of tetragonal Cu_4O_3 seems to become more prominent (Fig. 3b). However, a strong intensity peak revealed the monoclinic CuO NPs highly polycrystalline character, which is shown to be higher in the TDCO3 sample. The Willamson Hall plot (W-H plot) was used to calculate the crystalline size and

microstrain for the synthesized samples (Fig. 4), as per Eq. (4). Nevertheless, the W-H approach was chosen for this investigation because it calculates the crystallite size with greater accuracy than the Scherrer method and takes into consideration both the broadening of the XRD peak caused by the lattice strain and the broadening that is dependent on the crystallite size (Vijayaprasath et al. 2016; Kumar et al. 2021; Naik et al. 2021).

$$\beta_O.\cos\theta = \frac{K\lambda}{D} + \beta_\varepsilon.\sin\theta \tag{4}$$

$$\beta_O = \beta_D + \beta_\varepsilon \tag{5}$$

Here, $\beta\cos\theta$ is plotted against $4\sin\theta$ for all synthesized TDCO1, TDCO3, and TDCO5 NPs which is displayed in Fig. 4a–c. As the slope (m) and y-intercept (c) values of the straight-line equation, $y = mx + c$ (linear fitted line), give the crystal strain (ε) and crystallite size (D), respectively (Xue et al. 2018; Shelke et al. 2022). The estimated crystallite size was 42.6, 42.1 and 48.9 nm for TDCO1, TDCO3, and TDCO5 NPs. Since the broadening caused by the microstrain is taken into account, the calculated D values will be considerably higher than the Scherrer method, whereas calculated microstrain (ε) values were 2.12, 7.54, and 1.07 $\times 10^{-3}$ for TDCO1, TDCO3, and TDCO5 NPs. The estimated microstrain values for the nanoparticles and their corresponding actual crystallite size are inversely related. The synthesized NPs crystal size is decreased owing to the flavonoids available in the leaf extract which functioned as a natural bio-reductant and capping agent (Samari et al. 2019). Typically, the smaller crystalline size allows for a greater possibility of adhesion to the negatively charged cell wall and can accelerate the cell lysis process.

FT-IR spectrum analysis

FT-IR spectroscopy was conducted to identify the bio-reductant that was specifically attached to the CuO NPs surface. The Fourier transform infrared spectra of green synthesized TDCO1, TDCO3, and TDCO5 NPs in the 4000–400 cm^{-1} region are shown in Fig. 5a–c using the KBr pellet method. The FT-IR spectrum of TDCO1 NPs shows the characteristic peak at 3388, 2842, 2343, 1630, 1381, 1119, 883, and 489 cm^{-1} (Fig. 5a). The broad intense peak around 3388 and 1630 cm^{-1} is consistent with the -OH stretching and bending vibrations of absorbed water molecules by the synthesized NPs (Daphedar and Taranath 2018). The peak at 2924 cm^{z-1} indicates the asymmetric -CH stretching vibration and that of corresponding -CH symmetric stretching was found at 2842 cm^{-1} (Ghasemi et al. 2020). The peak 2343 cm^{-1} was assigned to the CO_2 absorption (Singh et al. 2019), similarly observed in the FT-IR spectrum of TDCO3 and TDCO5 samples. The peak appeared at 1119 cm^{-1} attributed to the stretching frequency of C-O. The 883 cm^{-1} absorption peak corresponds to the C=C bending vibration

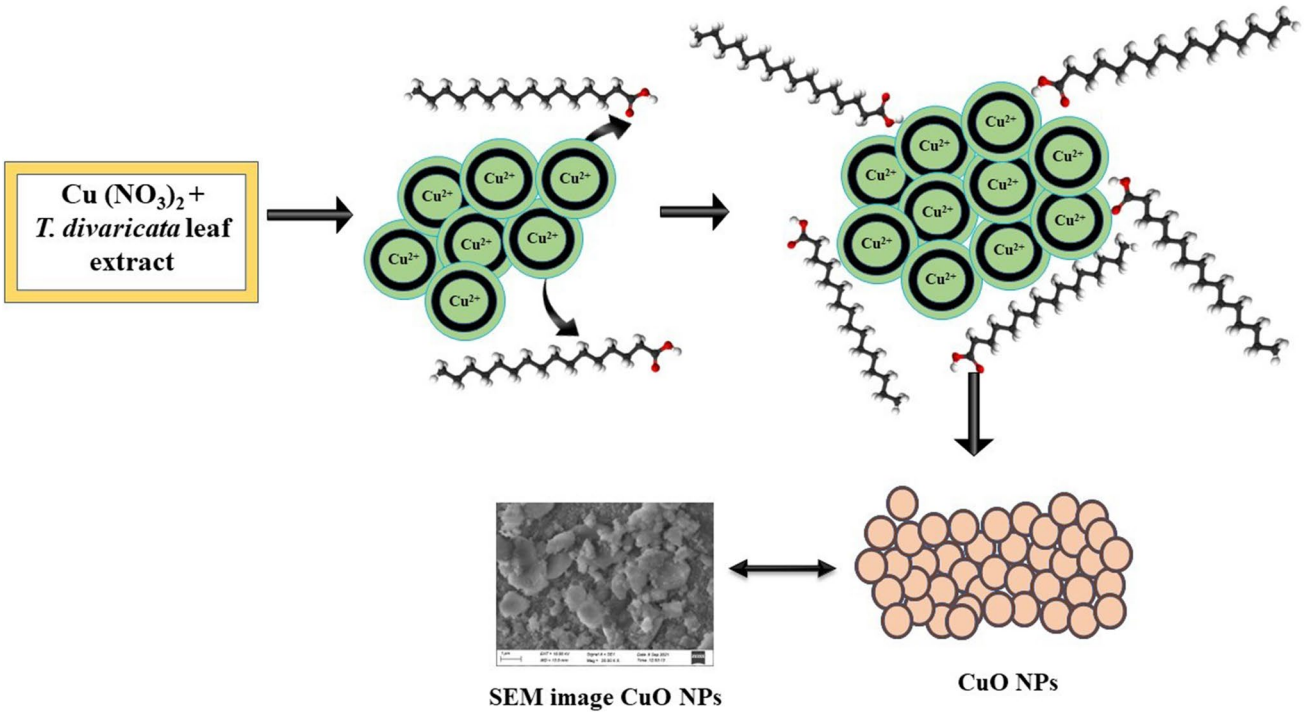

Fig. 2 Mechanism for the capping and reducing behaviour of phytochemicals in CuO NPs formation

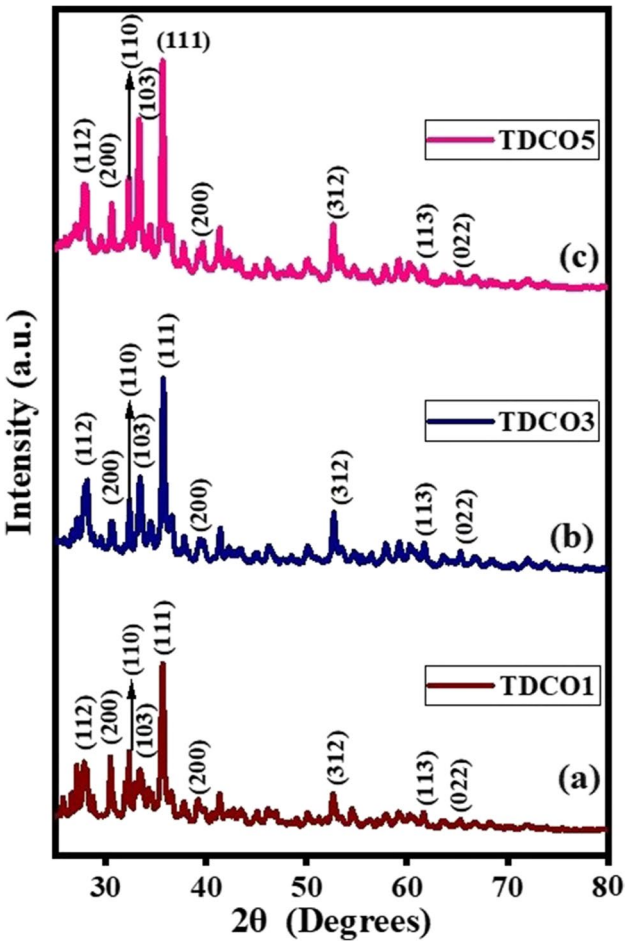

Fig. 3 X-ray diffraction pattern of TDCO1 (**a**), TDCO3 (**b**), and TDCO5 (**c**) NPs

of alkene, confirming 3, 7, 11, and 15-tetramethyl-2-hexadecane-1-ol presence.

These phytochemical-contained functions serve as effective reducing, capping, and precipitating agents for the synthesis of NPs. The metal oxides are responsible for the absorption peak within the 600 and 300 cm^{-1} range (Jagathesan and Rajiv 2018). The absorption band observable at 489 cm^{-1} was assigned to the Cu-O bond confirming the formation of CuO NPs. All the characteristic peaks observed above for TDCO1 NPs are similar to the FT-IR spectrum of TDCO3 and TDCO5 NPs (Fig. 5b and c). TDCO3 NPs Cu-O stretching band shown in Fig. 5b, however, exhibits a minor shift towards a lower wavenumber at 478 cm^{-1} resembling a change in NPs size which is consistent with the demonstrated XRD findings.

Surface morphology elucidation by SEM analysis

The scanning electron microscopy (SEM) analysis at two distinct magnifications, 1 µm and 200 nm, for the synthesized TDCO1, TDCO3, and TDCO5 NPs revealed the surface morphology, particle size, and distribution (Fig. 6). The size of the grains in the synthesized NPs decreased as a consequence of the bio-reductants phytol and n-hexadecanoic acid. It is interesting to observe that the *T. divaricate* leaf extract not only functioned as a capping agent but also as a reducing agent by providing -OH and -CO groups, which reduced particle size (Shayegan Mehr et al. 2018; Vasantharaj et al. 2019). It is noted that TDCO1 and TDCO3 NPs displayed in Fig. 6a–d has oval- and round-shaped grains with smooth surface. However, once the concentration of copper (Cu-5g) increases, the grain also starts to expand unevenly and the surface morphology appears to be more agglomerated (Fig. 6e and f), which was clearly seen for TDCO5 NPs.

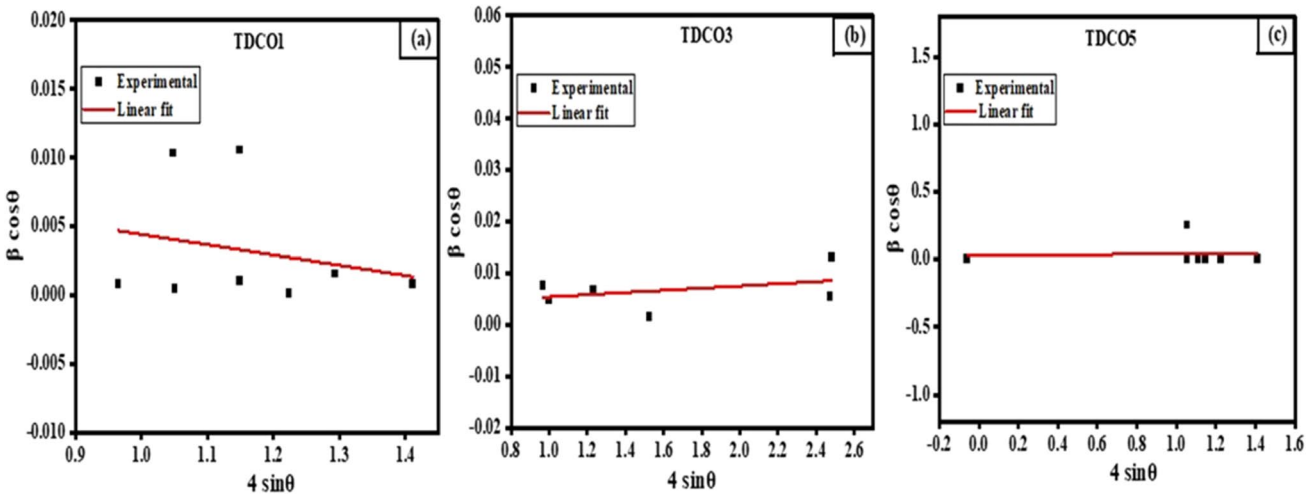

Fig. 4 W-H plot of (**a**) TDCO1, (**b**) TDCO3, and (**c**) TDCO5 NPs

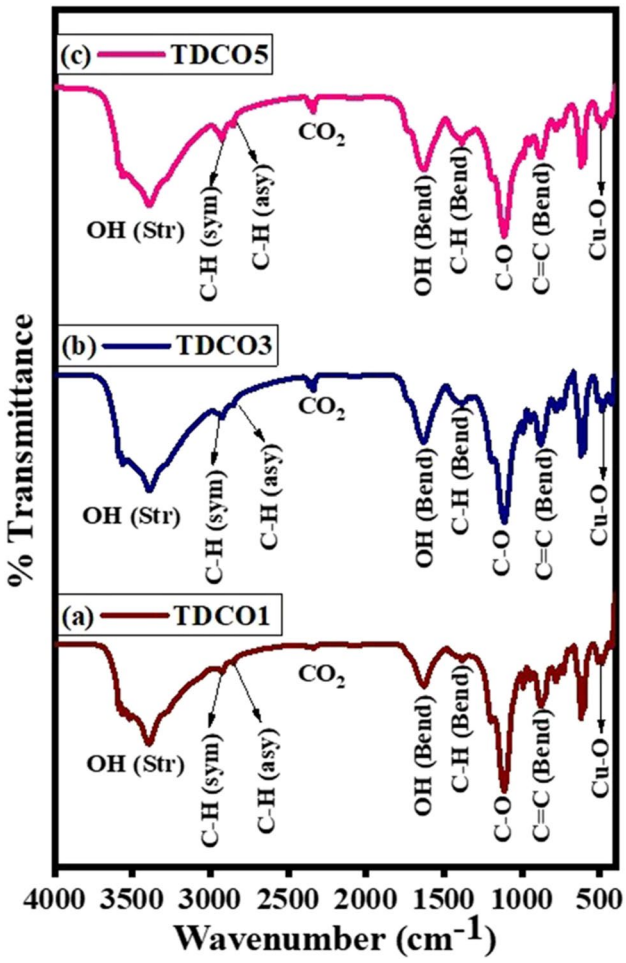

Fig. 5 FT-IR spectrum of TDCO1 (**a**), TDCO3 (**b**), and TDCO5 (**c**) NPs

The chemical composition of the prepared TDCO3 NPs was analyzed through EDAX analysis; the consequences of which are shown in Fig. 7. Figure 7a clearly revealed the presence of only Cu and O elements without any impurities in the TDCO3 NPs. To further verify the presence of these two elements, we conducted EDAX elemental mapping analysis, which is shown in Fig. 7b. This analysis further confirmed the presence of copper and oxygen elements in the TDCO3 NPs.

Antimicrobial activity

The synthesized TDCO1, TDCO3, and TDCO5 effective bacterial inhibition properties were tested against two basic pathogens, namely, *K. pneumoniae* as a gram-negative (G^-) and *B. subtilis* as a gram-positive (G^+) strain. Interestingly, *K. pneumoniae* (G^-) is a rod-like-shaped thick cell walled (thickness = 160 nm) bacillus that belongs to the family Enterobacteriaceae and the genus *Klebsiella*. *K. pneumoniae* is an enteric bacterium found in 5% of healthy human digestive tracts and may also live in the mouth and skin (Doorduijn et al. 2016). Although there are few cases of infections occurring naturally, *K. pneumoniae* can cause pneumonia in guinea pigs and other living organisms (Amako et al. 1988). The photographic images of *K. pneumoniae* cultured on Petri dishes which was treated with varying concentrations of NPs (40, 50, and 60 µg/mL) are displayed in Fig. 8a–c.

B. subtilis (G^+) is a rod-shaped bacterium having a single lipid bilayer membrane that serves as a permeability barrier with a thick cell wall (thickness = 33 nm). It is found commonly in soil and is regarded as a non-pathogenic bacterium (Dadd and Paulton 1968). The *B. subtilis* bacteria inoculated with varying concentrations of synthesized NPs (40, 50, and 60 µg/mL) are shown in Fig. 8d–f. Table 1 shows that the inhibited zone (IZ) results encounter an elevated value whenever the test material concentration increases which reveals information about the synthesized CuO NPs dose-dependent activity. The bar diagram representation (Fig. 9a and b) justifies that TDCO3 NPs delivered better-inhibited zone values than the other two NPs; here, well-known antibiotic amoxicillin was utilized as a positive control for both bacterial strains. Based on previous studies, we suggested a hypothesis for the enhanced antimicrobial activity of synthesized NPs (Mendes et al. 2022). G^- bacteria contain a thin layer between two membranes of peptidoglycan which is responsible for its good antibacterial resistance. Additionally, the membranes dissociated carboxyl groups causing the cell surface to charge negatively. Contrarily, CuO NPs have a positive charge because of the positive charges of the Cu^{2+} ions and the electrostatic gradient variations across the negative membrane that could severely damage the cell membrane. Subsequently, negative charges on the cell surface are due to the lipoteichoic acid in the membrane and the teichoic acid in the peptidoglycan layer (Ahmed et al. 2021). Teichoic and lipoteichoic acids chelate Cu^{2+} ions which are then transported across membrane proteins by passive diffusion.

As already known, CuO is a transition metal oxide and semiconductor with a broadband gap (3.25 eV) and electron-hole pairs are created when the radiation energy exceeds the CuO band gap. The produced electrons are promoted to the conduction band (CB) and significantly an oxidizing character is acquired by the hole that is produced in the valence band (VB) which oxidizes water molecules or hydroxide anions and produces powerful oxidizing species (Kumar et al. 2019; Abdo et al. 2021). Furthermore, CuO in its Cu^{2+} form severely damages the cytoplasmic membrane, due to its particular affinity for sulfur, and the Cu^{2+} ion inhibits the glycolytic enzyme by oxidizing thiol groups (Fig. 10). Importantly, bacterial cell division is a complicated and dynamic process that begins with the polymerization of the FtsZ protein in order to build the

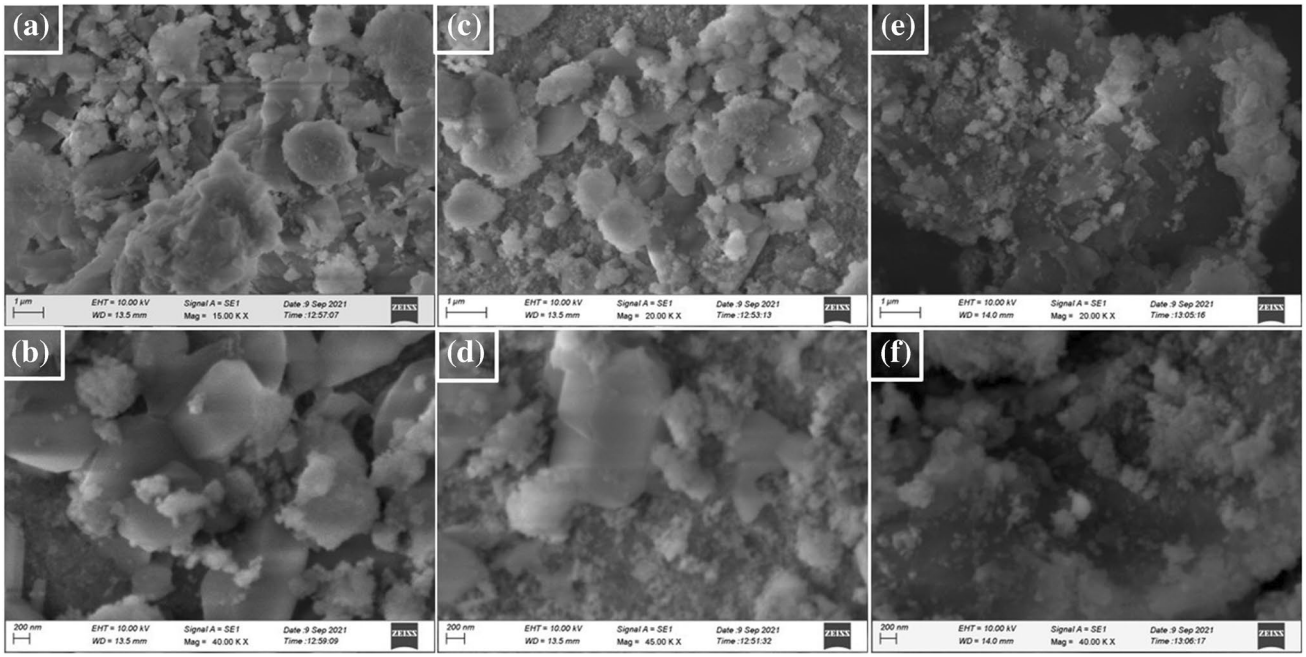

Fig. 6 SEM images at two different magnifications 1 µm and 200 nm of TDCO1 (**a** and **b**), TDCO3 (**c** and **d**), and TDCO5 (**e** and **f**) NPs

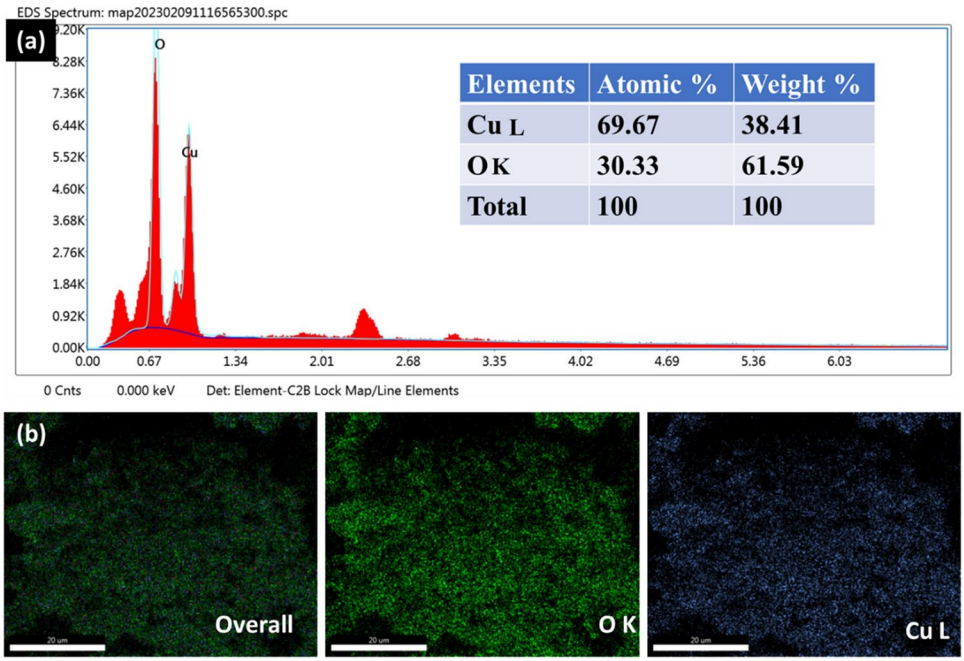

Fig. 7 (**a**) EDAX spectra and (**b**) elemental mapping analysis of TDCO3 NPs

divisome which will control all the processes involved in cell division as well as the production and remodelling of the cell wall (Gnanasekaran et al. 2021). CuO NPs work by stopping FtsZ-GTPase activity which in turn induces cell filamentation stops cell division and promotes cell lysis. According to previously published papers, the antibacterial activity of the as-prepared TDCO3 nanoparticles was compared and is shown in Table 2.

In vitro anticancer analysis (HeLa cell)

The synthesized TDCO1, TDCO3, and TDCO5 NPs anticancer activity was assessed against the HeLa cell line which is

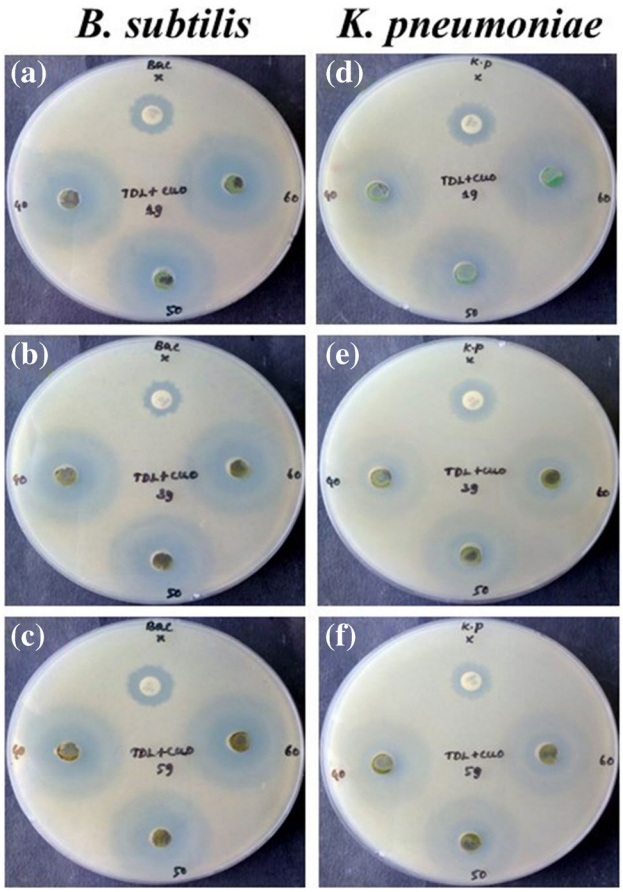

Fig. 8 Antibacterial activity for TDCO1, TDCO3, and TDCO5 NPs with amoxycillin against (G^+) *B. subtilis* (**a**–**c**) and (G^-) *K. pneumoniae* (**d**–**f**) bacterial strains

displayed in Fig. 11. This study was assessed with varying concentration (0, 5, 10, 25, 50, and 100 µg/mL^{-1}) of the test material. Hereby, the anticancer results presented in the form of bar diagram suggested that TDCO1 (Fig. 12a) shows 99.4, 81.2, 62.5, 47.1, 33.2, and 24.3 %, TDCO3 exhibits 99.5, 71.4, 56.8, 41.2, 35.6, and 27.2%, and TDCO5 delivered 98.2, 81.2, 62.5, 47.1, 33.2, and 24.3% of cell lysis corresponding to 0, 5, 10, 25, 50, and 100 µg/mL^{-1} concentration. The percentage cell viability was evaluated to be minimal at 100 µg/mL^{-1} dose concentration for all the synthesized CuO NPs. Moreover, the IC_{50} values were found by taking linear regression which suggested that TDCO3 demonstrated a lower IC_{50} value of about 18.2 µg/mL^{-1} than TDCO1 (IC_{50} = 21.5 µg/mL^{-1}) and TDCO5 (IC_{50} = 19.6 µg/mL^{-1}) NPs (Fig. 12b). The key mechanisms underpinning TDCO3 NPs improved cytotoxicity and increased activity were ROS production to be the production of ROS, oxidative stress, and the activation of apoptosis, all of which play a crucial role in the death of HeLa cancer cells (Arumugam et al. 2021).

The crystalline size, surface shape, surface charge distribution, test material dose, and dissolution kinetics of CuO NPs are some examples of physical characteristics that play a crucial role in the cytotoxic effect. The cytotoxic effects of TDCO3 NPs are more prominent due to their small size (12.1 nm), and they can easily enter HeLa cells to create the ROS that causes cell death. Figure 10 depicts the process through which CuO NPs cause cytotoxicity due to the evenly distributed CuO NPs that enter into the cells easily and kill the HeLa cancer cells. Another significant factor in the lethality of HeLa cancer cells is the surface charge. Owing to the Vander walls interaction between negatively charged cell membranes, positive charged Cu^+, and Cu^{2+} ions could cause greater harm than negative charges (Pandiyan et al. 2019; Ansari and Asiri 2021). The attraction of the positively charged CuO NPs to the negatively charged cell membrane is what causes this charging effect. The CuO NPs interact with the negatively charged surface of cancer cells, causing cell membrane leakage and making cancer cells more hazardous (Mousavi-Kouhi et al. 2021). Additionally, the dissolving Cu^+ and Cu^{2+} ions will cause effective cytotoxicity, which will cause the enzyme system to be disrupted. As a result, CuO NPs synthesized by *T. divaricate* leaf extract had excellent anticancer activity against HeLa cells. Utilizing plant extracts also has the advantages of being secure and environmentally beneficial. Finally, CuO NPs have the potential to function as a more potent and effective anticancer therapeutic agent.

In vitro anti-inflammatory analysis

The synthesized TDCO3 NPs anti-inflammatory activity was assessed through the BSA denaturation technique, and the bar diagram representing percentage inhibition at different

Table 1 Zone of inhibition (ZI) value for TDCO1, TDCO3, and TDCO5 NPs against (G^+) *B. subtilis* (a) and (G^-) *K. pneumoniae* (b) pathogens

S. No.	Sample code	Zone of Inhibition (mm)					
		B. subtilis (G^{+ve})			*K. pneumoniae* (G^{-ve})		
		40 µg/mL	50 µg/mL	60 µg/mL	40 µg/mL	50 µg/mL	60 µg/mL
1.	TDCO1	31.5	32	34	29	29.5	30
2.	TDCO3	33.5	34	34	29.5	32	33
3.	TDCO5	31	32	32.5	29	29	29.5

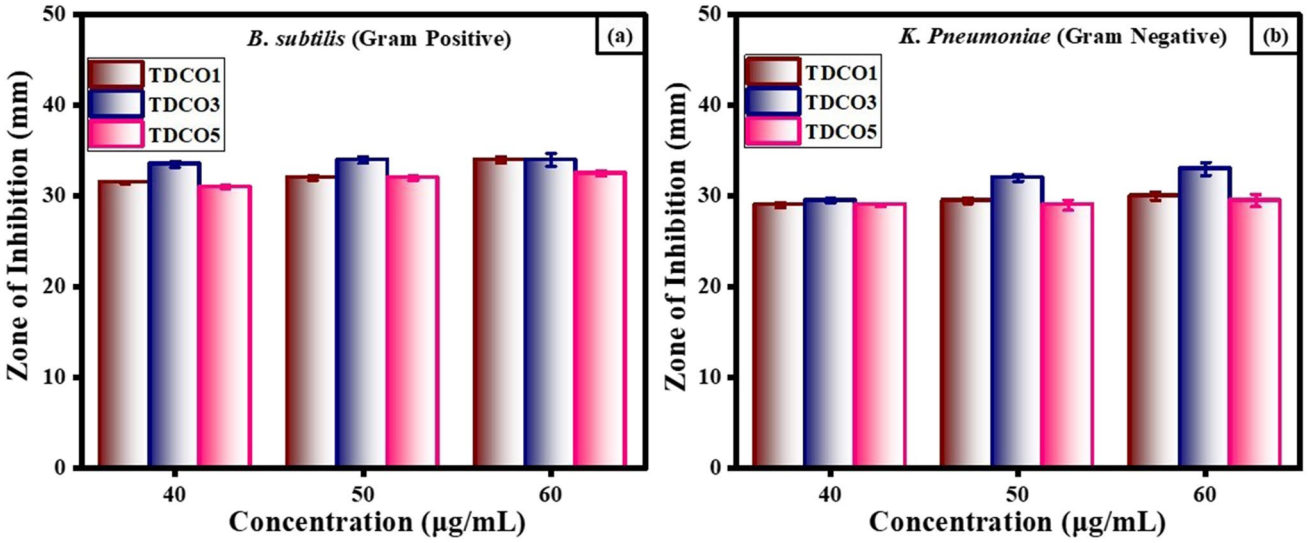

Fig. 9 Bar diagrammatic representation of zone of inhibition for TDCO1, TDCO3, and TDCO5 NPs against (G^+) *B. subtilis* (**a**) and (G^-) *K. pneumoniae* (**b**) bacterial strains

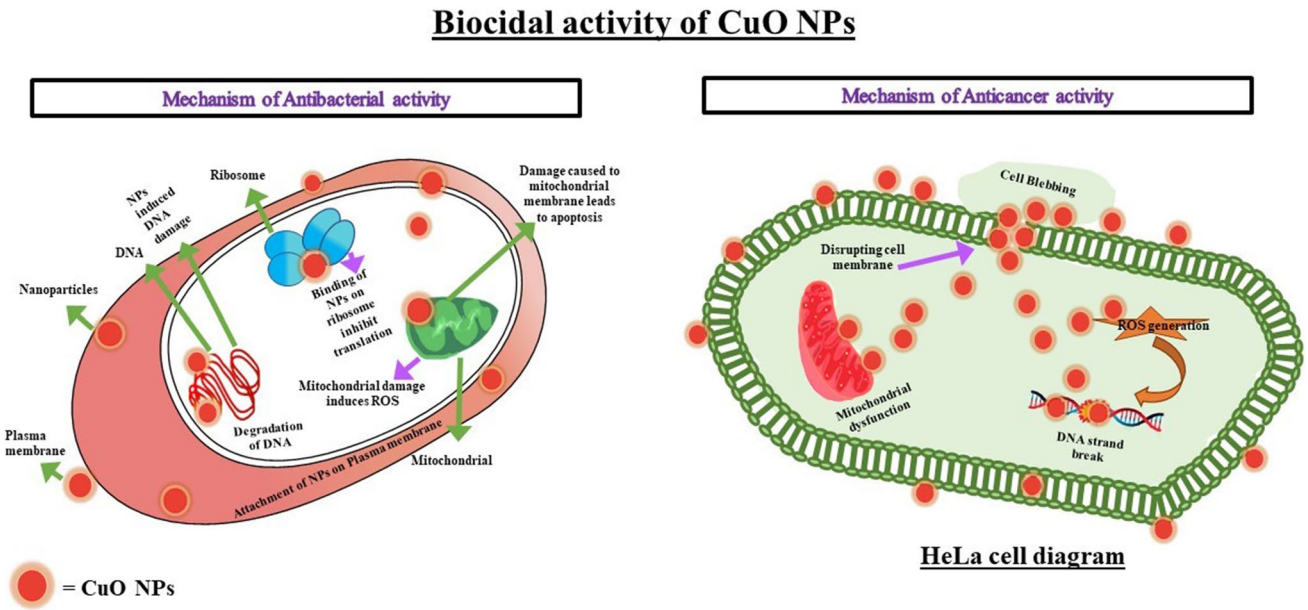

Fig. 10 Graphical representation of antibacterial and anticancer activity of CuO NPs

NPs dosages is displayed in Fig. 12c. Moreover, the TDCO3 NPs were supplemented at five different concentrations 10, 50, 100, 250, and 500 µg/mL; similarly, Diclofenac sodium was also performed. The values obtained for TDCO3 NPs were 20.11, 40.27, 52.44, 65.83, and 85.66% for 10, 50, 100, 250, and 500 µg/mL concentrations. The percentage inhibition acquired for Diclofenac sodium (standard) was at 22.33, 45.67, 70.08, 58.67, and 95.55% for 10, 50, 100, 250, and 500 µg/mL, respectively. Besides, the anti-inflammatory activity was observed maximum of 85.66% for the highest concentration of 500 µg/mL. The obtained inhibition percentage was close to Diclofenac sodium which showed 95.55% at 500 µg/mL concentration. Protein denaturation is a general process that results in the loss of biological activity by degrading secondary and tertiary protein structures (Muthulakshmi and Sundrarajan 2020). A variety of factors, including salts or alcohol, might change the solubility of albumin. In contrast to infectious activity like antibacterial activity, it is attractive to assess the defensive action like an anti-inflammatory potential (Veerasingam et al. 2020;

Table 2 Comparison of antimicrobial activity test results for various nanoparticles

S. No.	Samples	Test of organism	Zone of inhibition (mm)	References
1	CdO-MgO nanocomposite	*K. pneumoniae*	13	Karthik et al. (2019)
2	NiO-CeO_2-ZnO nanocomposite	*E. coli*	13	Subhan et al. (2015)
3	CuO nanoparticles	*E. coli*	08	Arunadevi et al. (2018)
4	CeO_2/CdO nanosphere	*K. pneumoniae*	08	Magdalane et al. (2016)
5	TiO_2 nanoparticles	*K. pneumoniae*	10.2	Subhapriya and Gomathipriya (2018)
6	MgO	*B. subtilis*	26	Palanisamy and Pazhanivel (2017)
7	ZnS/Ag/$CoFe_2O_4$ nanocomposite	*E. coli*	26	Palanisamy et al. (2020)
8	TDCO3	*K. pneumoniae*	32	Present work
		B. subtilis	34	

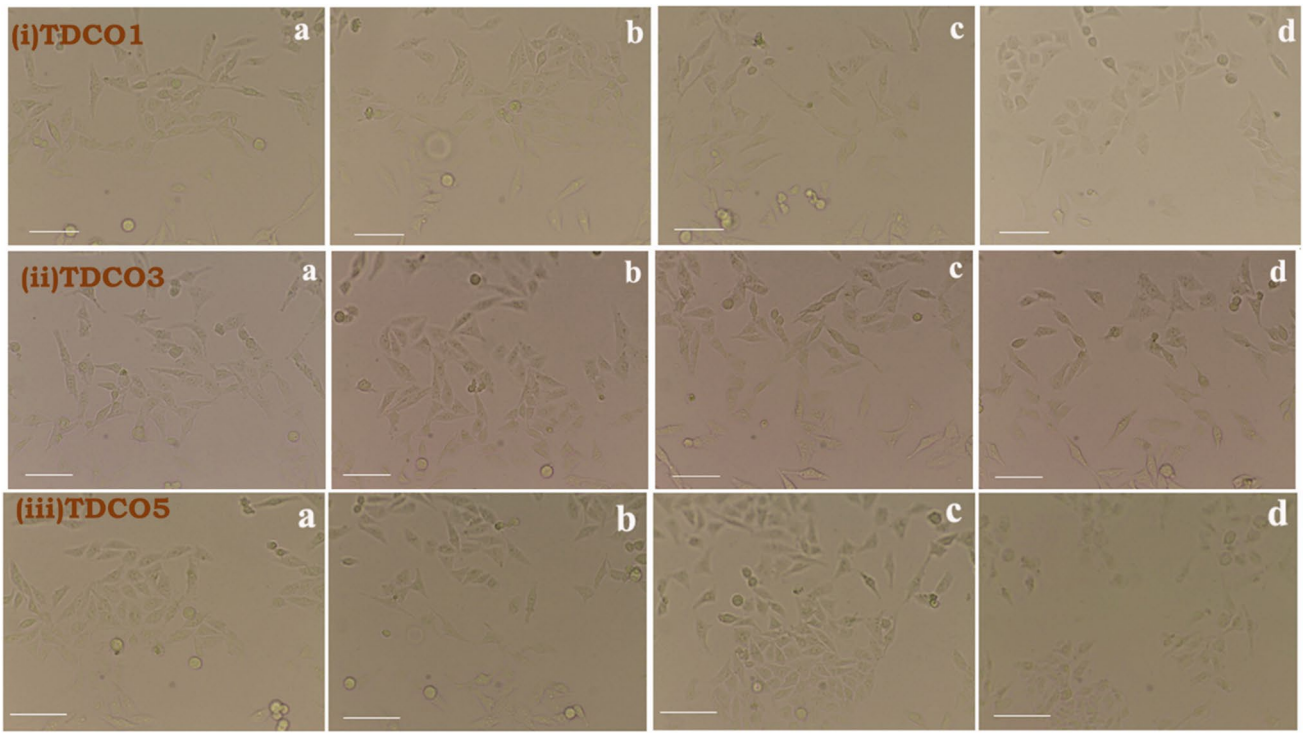

Fig. 11 Optical microscope images of Hela cells inoculated with different concentrations (0, 5, 10, 25, 50, and 100 μg/mL^{-1}) of TDCO1 (i), TDCO3 (ii), and TDCO5 (iii) NPs

Velsankar et al. 2020a). This analysis demonstrated high inhibition towards BSA denaturation which in turn expressed that TDCO3 NPs functioned as an effective anti-inflammatory drug.

In vitro anti-diabetic drug

The most prevalent condition affecting persons between the ages of 40 and 60 is diabetes mellitus, which is brought on by insufficient insulin production and rising blood glucose levels. Anti-diabetic medications are taken to treat diabetes and manage insulin shortage (Nasab et al. 2020; Sundrarajan and Muthulakshmi 2021). Numerous studies have been done to identify viable anti-diabetic medications (Kazmi et al. 2021). In this current research, we have aimed to figure out whether TDCO3 NPs could function as an effective anti-diabetic drug via inhibiting α-amylase with a standard drug as "acarbose." The bar diagrammatic representation of percentage inhibition versus

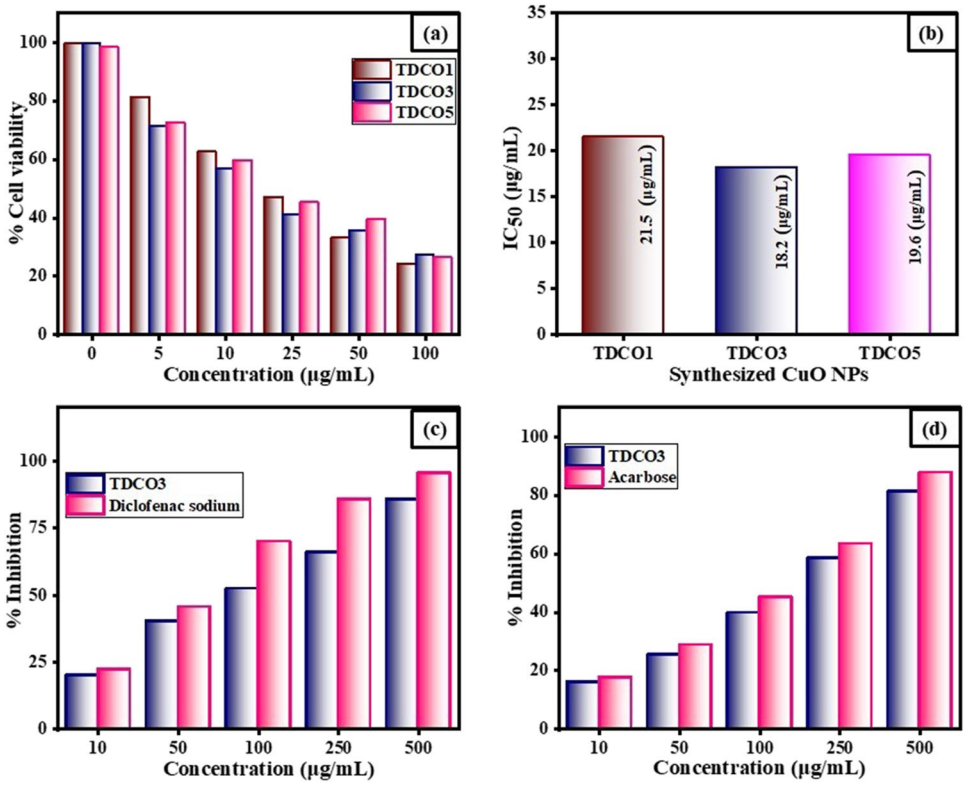

Fig. 12 Bar diagram representation of anticancer activity (**a**), IC_{50} value of TDCO1, TDCO3, and TDCO5 NPs, anti-inflammatory activity (**c**), and anti-diabetic activity of TDCO3 NPs

TDCO3 and acarbose concentration (10–500 µg/ml) is shown in Fig. 12d. Notably, at a higher concentration of 500 µg/ml TDCO3 NPs and acarbose exhibited maximum scavenging activity as 81.18 and 87.71% as inhibition percentage, respectively. Moreover, the obtained anti-diabetic results suggested that TDCO3 NPs delivered scavenging activity close to the standard acarbose and could be utilized as a potential anti-diabetic drug.

Conclusion

The *T. divaricate* leaf extract was successfully used to biosynthesize CuO NPs using inexpensive, environmentally responsible, and less dangerous chemical techniques. The development of monoclinic and tetragonal phases of CuO NPs with a crystallite size of 12.1 nm was suggested by the powder XRD pattern. The bands of functional groups involved in the Phyto-mediated green synthesis of CuO NPs, including Cu and O bonding, were visible in the FT-IR spectrum. The morphology of the CuO NPs seemed to be round and oval in the scanning electron micrographs. TDCO3 NPs exhibit excellent antibacterial and anticancer action compared to TDCO1 and TDCO5 NPs. The TDCO3 NPs have therefore functioned as a more potent drug against the *K. pneumoniae* (G^-) and *B. subtilis* (G^+) strains, and they ensured the HeLa cells were most significantly cytotoxic. The anti-inflammatory analysis revealed possible effective activity on egg albumin inhibition by TDCO3 NPs. Synthesized TDCO3 NPs anti-diabetic properties showed that they would work well as a medication to treat diabetes. We conclude that CuO NPs are a promising material for use in biomedical applications.

Author contributions Manonmani Raju: conceptualization; investigation; writing—original draft; visualization; Balaji Parasuraman: data curation; validation; investigation; formal analysis; Palanisamy Govindasamy: visualization; investigation, formal analysis; Pazhanivel Thangavelu: methodology; data curation; validation; formal analysis; Sasikumar Duraisamy: supervision; visualization; project administration; formal analysis

Data availability The datasets used and analyzed during the current study are available from the corresponding author on reasonable request.

Declarations

Ethics approval and consent to participate Not applicable.

Consent for publication Not applicable.

Conflict of interest The authors declare no competing interests.

References

Abdo AM, Fouda A, Eid AM et al (2021) Green synthesis of zinc oxide nanoparticles (ZnO-NPs) by Pseudomonas aeruginosa and their activity against pathogenic microbes and common house mosquito, Culex pipiens. Materials (Basel) 14(22):6983

Ahmed T, Wu Z, Jiang H et al (2021) Bioinspired green synthesis of zinc oxide nanoparticles from a native bacillus cereus strain rnt6: characterization and antibacterial activity against rice panicle blight pathogens burkholderia glumae and B. Gladioli. Nanomaterials 11:884. https://doi.org/10.3390/nano11040884

Amako K, Meno Y, Takade A (1988) Fine structures of the capsules of Klebsiella pneumoniae and Escherichia coli K1. J Bacteriol 170:4960–4962. https://doi.org/10.1128/jb.170.10.4960-4962.1988

Anand GT, Nithiyavathi R, Ramesh R et al (2020) Structural and optical properties of nickel oxide nanoparticles: investigation of antimicrobial applications. Surf Interfaces 18:100460. https://doi.org/10.1016/j.surfin.2020.100460

Ananda Murthy HC, Zeleke TD, Tan KB et al (2021) Enhanced multifunctionality of CuO nanoparticles synthesized using aqueous leaf extract of Vernonia amygdalina plant. Results Chem 3:100141. https://doi.org/10.1016/j.rechem.2021.100141

Ansari MA, Asiri SMM (2021) Green synthesis, antimicrobial, antibiofilm and antitumor activities of superparamagnetic γ-Fe_2O_3 NPs and their molecular docking study with cell wall mannoproteins and peptidoglycan. Int J Biol Macromol 171:44–58. https://doi.org/10.1016/j.ijbiomac.2020.12.162

Arumugam M, Murugesan B, Pandiyan N et al (2021) Electrospinning cellulose acetate/silk fibroin/Au-Ag hybrid composite nanofiber for enhanced biocidal activity against MCF-7 breast cancer cell. Mater Sci Eng C 123:112019. https://doi.org/10.1016/j.msec.2021.112019

Arunadevi R, Kavitha B, Rajarajan M et al (2018) Investigation of the drastic improvement of photocatalytic degradation of Congo red by monoclinic Cd, Ba-CuO nanoparticles and its antimicrobial activities. Surf Interfaces 10:32–44. https://doi.org/10.1016/j.surfin.2017.11.004

Dadd AH, Paulton RJ (1968) The cell wall of Bacillus subtilis during synchronous growth. J Gen Microbiol 53:539–596

Daphedar A, Taranath TC (2018) Green synthesis of zinc nanoparticles using leaf extract of Albizia saman (Jacq.) Merr. and their effect on root meristems of Drimia indica (Roxb.) Jessop. Caryologia 71:93–102. https://doi.org/10.1080/00087114.2018.1437980

Darvishi E, Kahrizi D, Arkan E (2019) Comparison of different properties of zinc oxide nanoparticles synthesized by the green (using Juglans regia L. leaf extract) and chemical methods. J Mol Liq 286:110831. https://doi.org/10.1016/j.molliq.2019.04.108

Doorduijn DJ, Rooijakkers SHM, van Schaik W, Bardoel BW (2016) Complement resistance mechanisms of Klebsiella pneumoniae. Immunobiology 221:1102–1109. https://doi.org/10.1016/j.imbio.2016.06.014

dos Santos AP, Belini GB, Mambrini GP et al (2019) Thermal degradation of calcium and sodium alginate: a greener synthesis towards calcium oxide micro/nanoparticles. Int J Biol Macromol 140:749–760. https://doi.org/10.1016/j.ijbiomac.2019.08.103

Ghasemi Z, Abdi V, Sourinejad I (2020) Single-step biosynthesis of Ag/AgCl@TiO_2 plasmonic nanocomposite with enhanced visible light photoactivity through aqueous leaf extract of a mangrove tree. Appl Nanosci 10:507–516. https://doi.org/10.1007/s13204-019-01149-4

Gnanasekaran L, Pachaiappan R, Kumar PS et al (2021) Visible light driven exotic p (CuO) - n (TiO_2) heterojunction for the photodegradation of 4-chlorophenol and antibacterial activity. Environ Pollut 287:117304. https://doi.org/10.1016/j.envpol.2021.117304

Gowri S, Gopinath K, Arumugam A (2018) Experimental and computational assessment of mycosynthesized CdO nanoparticles towards biomedical applications. J Photochem Photobiol B Biol 180:166–174. https://doi.org/10.1016/j.jphotobiol.2018.02.009

Hasnidawani JN, Azlina HN, Norita H et al (2016) Synthesis of ZnO nanostructures using sol-gel method. Procedia Chem 19:211–216. https://doi.org/10.1016/j.proche.2016.03.095

Jadhav MS, Kulkarni S, Raikar P et al (2018) Green biosynthesis of CuO & Ag-CuO nanoparticles from Malus domestica leaf extract and evaluation of antibacterial, antioxidant and DNA cleavage activities. New J Chem 42:204–213. https://doi.org/10.1039/c7nj02977b

Jagathesan G, Rajiv P (2018) Biosynthesis and characterization of iron oxide nanoparticles using Eichhornia crassipes leaf extract and assessing their antibacterial activity. Biocatal Agric Biotechnol 13:90–94. https://doi.org/10.1016/j.bcab.2017.11.014

Javed R, Ahmed M, Haq I et al (2017) PVP and PEG doped CuO nanoparticles are more biologically active: antibacterial, antioxidant, antidiabetic and cytotoxic perspective. Mater Sci Eng C 79:108–115. https://doi.org/10.1016/j.msec.2017.05.006

Jayakumarai G, Gokulpriya C, Sudhapriya R et al (2015) Phytofabrication and characterization of monodisperse copper oxide nanoparticles using Albizia lebbeck leaf extract. Appl Nanosci 5:1017–1021. https://doi.org/10.1007/s13204-015-0402-1

Jose Varghese R, Zikalala N, Sakho EHM, Oluwafemi OS (2020) Green synthesis protocol on metal oxide nanoparticles using plant extracts. Elsevier Inc.

Kainat KMA, Ali F et al (2021) Exploring the therapeutic potential of Hibiscus rosa sinensis synthesized cobalt oxide (Co_3O_4-NPs) and magnesium oxide nanoparticles (MgO-NPs). Saudi J Biol Sci 28:5157–5167. https://doi.org/10.1016/j.sjbs.2021.05.035

Kalaimagal C (2019) Identification of bioactive compounds in flower of Tabernaemontana divaricata (L.) using gas chromatography–mass spectrometry analysis. Asian J Pharm Clin Res 12:129–132. https://doi.org/10.22159/ajpcr.2019.v12i9.34559

Karthik K, Dhanuskodi S, Gobinath C et al (2019) Ultrasonic-assisted CdO–MgO nanocomposite for multifunctional applications. Mater Technol 34:403–414. https://doi.org/10.1080/10667857.2019.1574963

Kazmi Z, Safdar N, Chaudhry G et al (2021) Radical scavenging capability influences the multifarious therapeutic tendencies of phyto-engineered CuO nanostructures. J Inorg Organomet Polym Mater 31:3125–3136. https://doi.org/10.1007/s10904-021-01940-3

Khan F, Akhtar N, Jalal N et al (2019) Carbon-dot wrapped ZnO nanoparticle-based photoelectrochemical sensor for selective monitoring of H_2O_2 released from cancer cells. Microchim Acta 186:1–9. https://doi.org/10.1007/s00604-019-3227-x

Król A, Railean-Plugaru V, Pomastowski P, Buszewski B (2019) Phytochemical investigation of Medicago sativa L. extract and its potential as a safe source for the synthesis of ZnO nanoparticles: The proposed mechanism of formation and antimicrobial activity. Phytochem Lett 31:170–180. https://doi.org/10.1016/j.phytol.2019.04.009

Kumar PPNV, Shameem U, Kollu P et al (2015) Green synthesis of copper oxide nanoparticles using Aloe vera leaf extract and its antibacterial activity against fish bacterial pathogens. Bionanoscience 5:135–139. https://doi.org/10.1007/s12668-015-0171-z

Kumar SV, Bafana AP, Pawar P et al (2019) Optimized production of antibacterial copper oxide nanoparticles in a microwave-assisted synthesis reaction using response surface methodology. Colloids Surf A: Physicochem Eng Asp 573:170–178. https://doi.org/10.1016/j.colsurfa.2019.04.063

Kumar P, Inwati GK, Mathpal MC et al (2021) Defects induced enhancement of antifungal activities of Zn doped CuO

nanostructures. Appl Surf Sci 560:150026. https://doi.org/10.1016/j.apsusc.2021.150026
Li H, Yu B, Zhuang Z et al (2021) A small change in the local atomic environment for a big improvement in single-atom catalysis. J Mater Chem A 9:4184–4192. https://doi.org/10.1039/d0ta10823e
Magdalane CM, Kaviyarasu K, Vijaya JJ et al (2016) Photocatalytic activity of binary metal oxide nanocomposites of CeO_2/CdO nanospheres: investigation of optical and antimicrobial activity. J Photochem Photobiol B Biol 163:77–86. https://doi.org/10.1016/j.jphotobiol.2016.08.013
Mahendiran D, Subash G, Arumai Selvan D et al (2017) Biosynthesis of zinc oxide nanoparticles using plant extracts of Aloe vera and Hibiscus sabdariffa: phytochemical, antibacterial, antioxidant and anti-proliferative studies. Bionanoscience 7:530–545. https://doi.org/10.1007/s12668-017-0418-y
Mendes CR, Dilarri G, Forsan CF et al (2022) Antibacterial action and target mechanisms of zinc oxide nanoparticles against bacterial pathogens. Sci Rep 12:1–10. https://doi.org/10.1038/s41598-022-06657-y
Mirzaei H, Darroudi M (2017) Zinc oxide nanoparticles: biological synthesis and biomedical applications. Ceram Int 43:907–914. https://doi.org/10.1016/j.ceramint.2016.10.051
Mousavi-Kouhi SM, Beyk-Khormizi A, Amiri MS et al (2021) Silver-zinc oxide nanocomposite: from synthesis to antimicrobial and anticancer properties. Ceram Int. 47(15):21490–21497. https://doi.org/10.1016/j.ceramint.2021.04.160
Muthulakshmi V, Sundrarajan M (2020) Green synthesis of ionic liquid assisted ytterbium oxide nanoparticles by Couroupita guianensis abul leaves extract for biological applications. J Environ Chem Eng 8:103992. https://doi.org/10.1016/j.jece.2020.103992
Muthuvel A, Jothibas M, Manoharan C (2020) Effect of chemically synthesis compared to biosynthesized ZnO-NPs using Solanum nigrum leaf extract and their photocatalytic, antibacterial and in-vitro antioxidant activity. J Environ Chem Eng 8:103705. https://doi.org/10.1016/j.jece.2020.103705
Naik EI, Naik HSB, Swamy BEK et al (2021) Influence of Cu doping on ZnO nanoparticles for improved structural, optical, electrochemical properties and their applications in efficient detection of latent fingerprints. Chem Data Collect 33:100671. https://doi.org/10.1016/j.cdc.2021.100671
Narayanan M, Vigneshwari P, Natarajan D et al (2021) Synthesis and characterization of TiO_2 NPs by aqueous leaf extract of Coleus aromaticus and assess their antibacterial, larvicidal, and anticancer potential. Environ Res 200:111335. https://doi.org/10.1016/j.envres.2021.111335
Nasab SB, Homaei A, Karami L (2020) Kinetic of α-amylase inhibition by Gracilaria corticata and Sargassum angustifolium extracts and zinc oxide nanoparticles. Biocatal Agric Biotechnol 23:101478. https://doi.org/10.1016/j.bcab.2019.101478
Palanisamy G, Pazhanivel T (2017) Green synthesis of MgO nanoparticles for antibacterial activity. Int Res J Eng Technol 4(9):137–141
Palanisamy G, Bhuvaneswari K, Chinnadurai A et al (2020) Magnetically recoverable multifunctional ZnS/Ag/$CoFe_2O_4$ nanocomposite for sunlight driven photocatalytic dye degradation and bactericidal application. J Phys Chem Solids 138:109231. https://doi.org/10.1016/j.jpcs.2019.109231
Pandiyan N, Murugesan B, Sonamuthu J et al (2018) Facile biological synthetic strategy to morphologically aligned CeO_2/ZrO_2 core nanoparticles using Justicia adhatoda extract and ionic liquid: Enhancement of its bio-medical properties. J Photochem Photobiol B Biol 178:481–488. https://doi.org/10.1016/j.jphotobiol.2017.11.036
Pandiyan N, Murugesan B, Sonamuthu J et al (2019) [BMIM] PF 6 ionic liquid mediated green synthesis of ceramic SrO/CeO_2 nanostructure using Pedalium murex leaf extract and their antioxidant and antibacterial activities. Ceram Int 45:12138–12148. https://doi.org/10.1016/j.ceramint.2019.03.116
Patzschke CF, Boot-Handford ME, Song Q, Fennell PS (2021) Co-precipitated Cu-Mn mixed metal oxides as oxygen carriers for chemical looping processes. Chem Eng J 407:127093. https://doi.org/10.1016/j.cej.2020.127093
Rafique M, Sadaf I, Tahir MB et al (2019) Novel and facile synthesis of silver nanoparticles using Albizia procera leaf extract for dye degradation and antibacterial applications. Mater Sci Eng C 99:1313–1324. https://doi.org/10.1016/j.msec.2019.02.059
Raja A, Ashokkumar S, Pavithra Marthandam R et al (2018) Eco-friendly preparation of zinc oxide nanoparticles using Tabernaemontana divaricata and its photocatalytic and antimicrobial activity. J Photochem Photobiol B Biol 181:53–58. https://doi.org/10.1016/j.jphotobiol.2018.02.011
Rehana D, Mahendiran D, Kumar RS, Rahiman AK (2017) In vitro antioxidant and antidiabetic activities of zinc oxide nanoparticles synthesized using different plant extracts. Bioprocess Biosyst Eng 40:943–957. https://doi.org/10.1007/s00449-017-1758-2
Samari F, Baluchi L, Salehipoor H, Yousefinejad S (2019) Controllable phyto-synthesis of cupric oxide nanoparticles by aqueous extract of Capparis spinosa (caper) leaves and application in iron sensing. Microchem J 150:104158. https://doi.org/10.1016/j.microc.2019.104158
Sarmast MK, Salehi H (2016) Silver nanoparticles: an influential element in plant nanobiotechnology. Mol Biotechnol 58:441–449. https://doi.org/10.1007/s12033-016-9943-0
Sathiyavimal S, Vasantharaj S, Veeramani V et al (2021) Green chemistry route of biosynthesized copper oxide nanoparticles using Psidium guajava leaf extract and their antibacterial activity and effective removal of industrial dyes. J Environ Chem Eng 9:105033. https://doi.org/10.1016/j.jece.2021.105033
Sharmila G, Thirumarimurugan M, Sivakumar VM (2016) Optical, catalytic and antibacterial properties of phytofabricated CuO nanoparticles using Tecoma castanifolia leaf extract. Optik (Stuttg) 127:7822–7828. https://doi.org/10.1016/j.ijleo.2016.05.142
Shayegan Mehr E, Sorbiun M, Ramazani A, Taghavi Fardood S (2018) Plant-mediated synthesis of zinc oxide and copper oxide nanoparticles by using ferulago angulata (schlecht) boiss extract and comparison of their photocatalytic degradation of Rhodamine B (RhB) under visible light irradiation. J Mater Sci Mater Electron 29:1333–1340. https://doi.org/10.1007/s10854-017-8039-3
Shelke HD, Machale AR, Survase AA et al (2022) Multifunctional Cu_2SnS_3 nanoparticles with enhanced photocatalytic dye degradation and antibacterial activity. Materials (Basel) 15:3126. https://doi.org/10.3390/ma15093126
Shojaei S, Ali MS, Suresh M et al (2021) Dynamic placenta-on-a-chip model for fetal risk assessment of nanoparticles intended to treat pregnancy-associated diseases. Biochim Biophys Acta - Mol Basis Dis 1867:166131. https://doi.org/10.1016/j.bbadis.2021.166131
Singh TP, Chauhan G, Agrawal RK, Mendiratta SK (2019) In vitro study on antimicrobial, antioxidant, FT-IR and GC–MS/MS analysis of Piper betle L. leaves extracts. J Food Meas Charact 13:466–475. https://doi.org/10.1007/s11694-018-9960-8
Singh S, Gupta P, Meena A, Luqman S (2020a) Acacetin, a flavone with diverse therapeutic potential in cancer, inflammation, infections and other metabolic disorders. Food Chem Toxicol 145:111708. https://doi.org/10.1016/j.fct.2020.111708
Singh SP, Kumar S, Mathan SV et al (2020b) Therapeutic application of Carica papaya leaf extract in the management of human diseases. DARU, J Pharm Sci 28:735–744. https://doi.org/10.1007/s40199-020-00348-7
Sivaraj R, Rahman PKSM, Rajiv P et al (2014) Biogenic copper oxide nanoparticles synthesis using Tabernaemontana divaricate leaf extract and its antibacterial activity against urinary tract pathogen.

Spectrochim Acta - Part A Mol Biomol Spectrosc 133:178–181. https://doi.org/10.1016/j.saa.2014.05.048

Sodipo BK, Aziz AA (2016) Recent advances in synthesis and surface modification of superparamagnetic iron oxide nanoparticles with silica. J Magn Magn Mater 416:275–291. https://doi.org/10.1016/j.jmmm.2016.05.019

Subhan MA, Ahmed T, Uddin N et al (2015) Synthesis, characterization, PL properties, photocatalytic and antibacterial activities of nano multi-metal oxide NiO·CeO_2·ZnO. Spectrochim Acta - Part A Mol Biomol Spectrosc 136:824–831. https://doi.org/10.1016/j.saa.2014.09.100

Subhapriya S, Gomathipriya P (2018) Green synthesis of titanium dioxide (TiO_2) nanoparticles by Trigonella foenum-graecum extract and its antimicrobial properties. Microb Pathog 116:215–220. https://doi.org/10.1016/j.micpath.2018.01.027

Sundrarajan M, Muthulakshmi V (2021) Green synthesis of ionic liquid mediated neodymium oxide nanoparticles by Andrographis paniculata leaves extract for effective bio-medical applications. J Environ Chem Eng 9:104716. https://doi.org/10.1016/j.jece.2020.104716

Taghizadeh SM, Morowvat MH, Negahdaripour M et al (2021) Biosynthesis of metals and metal oxide nanoparticles through microalgal nanobiotechnology: quality control aspects. Bionanoscience 11:209–226. https://doi.org/10.1007/s12668-020-00805-2

Tanna JA, Chaudhary RG, Juneja HD et al (2015) Histidine-capped ZnO nanoparticles: an efficient synthesis, spectral characterization and effective antibacterial activity. Bionanoscience 5:123–134. https://doi.org/10.1007/s12668-015-0170-0

Umamaheswari G (2015) Research article Bioactive compounds from the leaves of Tabernaemontana divaricata (L .). 6:3520–3522

Vasantharaj S, Sathiyavimal S, Saravanan M et al (2019) Synthesis of ecofriendly copper oxide nanoparticles for fabrication over textile fabrics: characterization of antibacterial activity and dye degradation potential. J Photochem Photobiol B Biol 191:143–149. https://doi.org/10.1016/j.jphotobiol.2018.12.026

Veerasingam M, Murugesan B, Mahalingam S (2020) Ionic liquid mediated morphologically improved lanthanum oxide nanoparticles by Andrographis paniculata leaves extract and its biomedical applications. J Rare Earths 38:281–291. https://doi.org/10.1016/j.jre.2019.06.006

Velsankar K, Aswin Kumara RM, Preethi R et al (2020a) Green synthesis of CuO nanoparticles via Allium sativum extract and its characterizations on antimicrobial, antioxidant, antilarvicidal activities. J Environ Chem Eng 8:104123. https://doi.org/10.1016/j.jece.2020.104123

Velsankar K, Vinothini V, Sudhahar S et al (2020b) Green synthesis of CuO nanoparticles via Plectranthus amboinicus leaves extract with its characterization on structural, morphological, and biological properties. Appl Nanosci 10:3953–3971. https://doi.org/10.1007/s13204-020-01504-w

Vijayaprasath G, Murugan R, Asaithambi S et al (2016) Structural and magnetic behavior of Ni/Mn co-doped ZnO nanoparticles prepared by co-precipitation method. Ceram Int 42:2836–2845. https://doi.org/10.1016/j.ceramint.2015.11.019

Wang Z, Brouri D, Casale S et al (2016) Exploration of the preparation of Cu/TiO_2 catalysts by deposition-precipitation with urea for selective hydrogenation of unsaturated hydrocarbons. J Catal 340:95–106. https://doi.org/10.1016/j.jcat.2016.05.011

Waris A, Din M, Ali A et al (2021) A comprehensive review of green synthesis of copper oxide nanoparticles and their diverse biomedical applications. Inorg Chem Commun 123:108369. https://doi.org/10.1016/j.inoche.2020.108369

Xue Y, Yu G, Shan Z, Li Z (2018) Phyto-mediated synthesized multifunctional Zn/CuO NPs hybrid nanoparticles for enhanced activity for kidney cancer therapy: A complete physical and biological analysis. J Photochem Photobiol B Biol 186:131–136. https://doi.org/10.1016/j.jphotobiol.2018.07.004

Zhao L, Lu L, Wang A et al (2020) Nano-biotechnology in agriculture: use of nanomaterials to promote plant growth and stress tolerance. J Agric Food Chem 68:1935–1947. https://doi.org/10.1021/acs.jafc.9b06615